Physics and Chemistry of Minerals (2019) 46:815–825
https://doi.org/10.1007/s00269-019-01042-0

ORIGINAL PAPER

Short-range order in Li–Al tourmalines: IR spectroscopy, X-ray single crystal diffraction analysis and a bond valence theory approach

Yuliya Bronzova[1] · Miriam Babushkina[2] · Olga Frank-Kamenetskaya[1] · Oleg Vereshchagin[1] · Ira Rozhdestvenskaya[1] · Anatoly Zolotarev[1]

Received: 29 January 2019 / Accepted: 3 June 2019 / Published online: 12 June 2019

Abstract
The short-range order in Li–Al–(OH^-, F^-) tourmalines with ^{Y}[Li/Al] ≈ 1 and different Na/Ca ratio was investigated by means of bond valence theory, experimental IR spectroscopic data and the results of X-ray single crystal diffraction. The stability of the arrangements coordinating *W*- and *V*-crystallographic sites occupied by OH^-, F^- and O^{2-} ions was refined. A unified model of assignment of absorption bands in the IR spectra to the local arrangements (clusters) was suggested taking into account the first and the second OH^-coordination spheres. The types of local cation arrangements around the *W*- and *V*-anion sites, alongside with clusters ratio and their distribution were brought out. The short-range order in Li–Al tourmalines controlled not only by local restrictions of the bond valence theory, but also by the long-range order was described.

Keywords Li–Al tourmaline · Short-range ordering · Bond valence theory · Infrared spectroscopy · X-ray single crystal diffraction

Introduction

The tourmaline supergroup minerals are complex borosilicates, which occur in a wide variety of igneous, metamorphic and sedimentary rocks of different origin and composition, including granitic pegmatites.

Due to the occurrence in different rocks, the stability in a wide range of thermodynamic conditions and the compositional variability, tourmalines are very useful indicators of the evolution of their host rock composition (e.g., Kuzmin et al. 1979; Hallsworth and Chisholm 2008; van Hinsberg et al. 2011; Kuznetsova et al. 2011; Vdacný and Bacik 2015; Vereshchagin et al. 2018).

The crystal structure of tourmaline (sp. gr. *R*3*m*) has been widely studied (e.g., Buerger and Parrish 1937; Gorskaya et al. 1982; Ertl et al. 2002; Rozhdestvenskaya et al. 2005, 2007, 2008; Gatta et al. 2014; Bosi 2018; Vereshchagin et al. 2018). Due to numerous ion replacements, the general formula of tourmaline may be given as follows: $(^{[9]}X^{[6]}Y_3^{[6]}Z_6[^{[4]}T_6O_{18}][^{[3]}BO_3]_3V_3W$ (X = Na^+, Ca^{2+}, K^+, vacancy); Y = Li^+, Al^{3+} etc.; Z = Al^{3+} etc.; T = Si^{4+}, Al^{3+}, B^{3+}; B = B^{3+}; V (O3) = OH^-, O^{2-}; W (O1) = OH^-, F^-, O^{2-}).

Connections between long-range order (crystal structure) and short-range order (atomic clusters) in tourmalines are widely discussed (Bosi 2011; Skogby et al. 2012; Vereshchagin et al. 2014; Bosi et al. 2016; Bosi 2018). Stability of atom arrangements around the *W*, *V*-sites (3*Y*–*W* and (*Y* + 2*Z*)-*V* clusters) (Fig. 1) can be estimated by the bond valence approach which was extended onto tourmaline by Hawthorne (1996, 2002) and Bosi (2011, 2018). For describing the short-range order in tourmaline structures, larger-sized clusters were suggested: $WY_3V_3Z_6$ (Bosi 2011) and (*W*)–(*YYY*)–[(*V*)(*V*)(*V*)]–(*ZZZZZZ*) (Watenphul et al. 2016; Bosi et al. 2016).

Vibrational spectroscopy can provide helpful information on local cation surroundings of OH^- ions in the tourmaline structure (e.g., Gebert and Zemann 1965; Nikolskaya and Samoylovich 1977; Kuzmin et al. 1979; Henry and Guidotti 1985; Gonzalez-Carreño et al. 1988; Mashkovtsev and Lebedev 1991; Castaneda et al. 2000; Skogby

✉ Yuliya Bronzova
paloma22@rambler.ru

Olga Frank-Kamenetskaya
ofrank-kam@mail.ru

[1] Saint Petersburg State University, Universitetskaya nab. 7/9, St. Petersburg 199034, Russia

[2] Institute of Precambrian Geology and Geochronology of Russian Academy of Sciences, nab. Makarova 2, St. Petersburg 199034, Russia

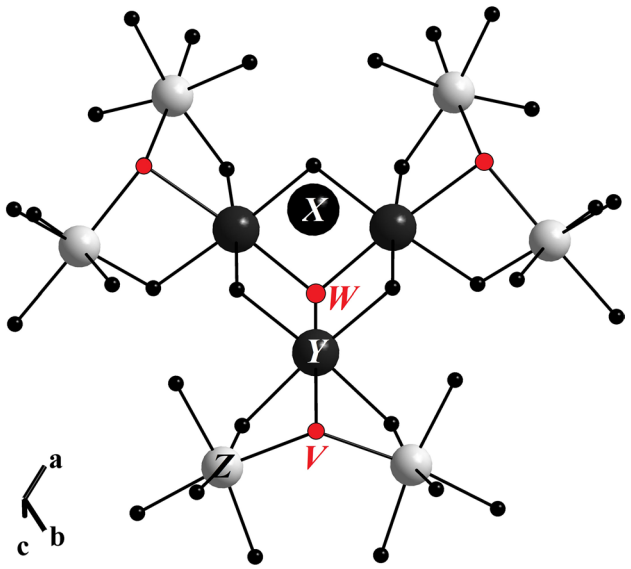

Fig. 1 Coordination of *W* and *V*-sites in tourmaline structure

et al. 2012; Fantini et al. 2013; Bosi et al. 2016; Watenphul et al. 2016). Skogby et al. (2012) suggested taking into account the stability of the coordinated arrangements around the *W, V*-sites (obtained by calculations using the bond valence theory) to increase the reliability of the band assignment in tourmaline IR spectra.

The IR studies carried out so far of Li–Al tourmalines (Table 1) provide different assignments of the absorption bands in the region of OH-group stretching vibration (3800–3000 cm^{-1}) with the specific local cation arrangements. In most publications dealing with IR spectroscopic studies of elbaite, including those containing Ca (e.g., Gonzalez-Carreño et al. 1988; Castaneda et al. 2000; Skogby et al. 2012; Fantini et al. 2013), bands of hydroxyl ion stretching vibration are assigned (as suggested in Gonzalez-Carreño et al. 1988) with three arrangements (clusters): ^{Y}(LiAlAl)–^{W}(OH^-), (^{Y}Li^{Z}Al^{Z}Al)–^{V}(OH^-), (^{Y}Al^{Z}Al^{Z}Al)–^{V}(OH^-). These kinds of assignments cannot be considered as reasonable, because no combinations of these arrangements enabled obtaining Li/Al ratio close to 1 in the YO_6 octahedron (which corresponds to elbaite composition). Mashkovtsev and Lebedev (1991) tried to overcome this problem by moving the boundary between high-frequency and low-frequency IR regions (Table 1), which allowed them to add one more coordinated arrangement ^{Y}(LiLiAl) around the OH-group in the *W*-site into account. Some authors (Gonzalez-Carreño et al. 1988; Fantini et al. 2013;

Table 1 Variants of assignment the OH^--ion stretching vibration bands (cm^{-1}) in the IR spectra of Ca-bearing Li–Al tourmalines with coordinating octahedral arrangements (according to literature data)

Interval of wavenumbers (cm^{-1})	Powder data					Single crystal data	
	Gonzalez-Carreño et al. (1988)		Mashkovtsev and Lebedev (1991)		Castaneda et al. (2000) (5 samples)	Skogby et al. (2012)	Fantini et al. (2013)
3680–3641	^{Y}(LiAlAl)–^{W}(OH) (3650)[a]	^{Y}(LiAlAl)–^{W}(OH) (3680) ^{Y}(LiAlAl)–^{W}(OH) (3651)	^{Y}(LiLiAl)–^{W}(OH) (3652)	^{Y}(LiLiAl)–^{W}(OH) (3652)	^{Y}(LiAlAl)–^{W}(OH)/ ^{Y}(AlAlAl)–^{W}(OH) (3647–3641)	^{Y}(LiAlAl)–^{W}(OH) (3657)	^{X}vac–^{W}(OH) (3660)
3604–3580	^{Y}Li^{Z}Al^{Z}Al–^{V}(OH) (3583)	^{Y}Li^{Z}Al^{Z}Al–^{V}(OH) (3604) ^{Y}Li^{Z}Al^{Z}Al–^{V}(OH) (3586)	^{Y}(LiAlAl)–^{W}(OH) (3580)	^{Y}(LiLiAl)–^{W}(OH)/ ^{Y}(LiAlAl)–^{W}(OH) (3610) ^{Y}(LiAlAl)–^{W}(OH) (3584)	^{Y}Li^{Z}Al^{Z}Al-^{V}(OH)/ ^{Y}Al^{Z}Al^{Z}Al-^{V}(OH) (3582-3580)	^{Y}Li^{Z}Al^{Z}Al-^{V}(OH) (3586)	^{Y}Li^{Z}Al^{Z}Al-^{V}(OH) (3593)
3566–3457	^{Y}Al^{Z}Al^{Z}Al–(OH)^{V} (3464)	^{Y}Al^{Z}Al^{Z}Al–^{V}(OH) (3507) ^{Y}Al^{Z}Al^{Z}Al–^{V}(OH) (3473)	^{Y}Li^{Z}Al^{Z}Al–^{V}(OH) (3460)	^{Y}Li^{Z}Al^{Z}Al–^{V}(OH)/^{Y}Al^{Z}Al^{Z}Al–^{V}(OH) (3506) ^{Y}Li^{Z}Al^{Z}Al–^{V}(OH)/^{Y}Al^{Z}Al^{Z}Al–^{V}(OH) (3462)	^{Y}Li^{Z}Al^{Z}Al–^{V}(OH)/ ^{Y}Al^{Z}Al^{Z}Al–^{V}(OH) (3460–3457)	^{Y}Al^{Z}Al^{Z}Al-^{V}(OH) (3475)	^{X}Na–^{V}(OH) (3566) ^{Y}Al^{Z}Al^{Z}Al–^{V}(OH) (3481)
3380–3170	O3–H···O5 (3335)	O3–H···O5 (3340)	O3–H···O5 (3380)	O3–H···O5 (3380)	H_2O (3340-3170)	O3–H···O5 (~3380)	No data
CaO content wt%	0.28	3.37	1.21	2.68	0.05-0.41	~ 0.29	0.29

[a]In brackets the location of the OH^- band in the IR spectrum is indicated

Bosi et al. 2016) attempted to assess the effect of not only the octahedral cations at the *Y*, *Z*-sites (the first coordinated OH^--ion sphere) but also of both cations and vacancies at the *X*-site (the second coordinated OH^--ion sphere) on the IR spectra of tourmalines. Skogby's assignment model for elbaite implies a local order distribution of two clusters ^{Y}(LiAlAl)–^{W}(OH^-), ^{Y}(LiLiAl)–^{W}(F^-) which are available in a certain ratio determined by *W*-site occupancy. This approach allows the Li/Al ratio in the YO_6 octahedron to be close to 1, while being inconsistent with the bond valence theory: according to the latter, the stabilities of ^{Y}(LiLiAl)–^{W}(F^-) and ^{Y}(LiLiAl)–^{W}(OH^-) arrangements are similar (Hawthorne 2002), which excludes an opportunity to give preference to only one of them. Overall, it needs to be stated that there is no reliable model for assigning absorption bands in the region of OH^--ion stretching vibrations of Li–Al tourmaline IR spectra to the specific atomic arrangements.

The main goal of this article is to study short-range order in Li–Al– (OH^-, F^-) tourmalines (^{Y}[Li/Al ≈ 1]), which does not contradict with the long-range order and is controlled by the bond valence theory.

The particular tasks of this study included the following:

1. To refine the stability of atomic arrangements coordinating *W*- and *V*-sites occupied by OH^-, F^- and O^{2-} ions.
2. To propose a unified assignment model of absorption bands in the region of OH^--ion stretching vibrations in IR spectra of studied tourmalines, taking into account both the first and the second OH-coordination spheres.
3. To determine the types of short-range arrangements around the *W*- and *V*-sites (OH^- and F^- ions) in the structure of studied tourmalines, to analyze their ratio and distribution.

Approaches and methods

The short order in Li–Al tourmalines was studied by combining the data from the estimation of the stability of atomic arrangements around the *W*- and *V*-sites for joint interpretation in terms of the bond valence theory, and from the experimentally achieved information by means of IR spectroscopy accompanied by X-ray single crystal diffraction analysis.

Estimation of the stability of coordinated atomic arrangements around the *W*- and *V*-sites

The analysis of the coordinated atomic arrangements in Li–Al tourmalines around the *W*- and *V*-sites [clusters $3Y$–^{W}(OH^-, F^-, O^{2-}) and $(Y+2Z)$–^{V}(OH^-)] allowed to estimate their stability in terms of local valence balance according to the approach proposed by Hawthorne (2002). Cation–anion distances (D_{ij}) were calculated using Brown's Eq. (2002):

$$D_{ij} = R_0 - 0.37 * \ln s_{ij}, \quad (1)$$

where s_{ij} represents the local bond valence and R_0 represents the bond valence empirical parameter

The value s_{ij} was calculated depending on the content of the cation *i* in the cluster (ranging from 1/3 to 1), its valence (Li^+, Al^{3+}), and the valence of the anion *j* (OH^-, F^-, O^{2-}), following the valence sum rule (Pauling 1929). According to Hawthorne (2002) we used the value of bond valence sum of 1.05 or 1.15 *vu* for the *W*- and *V*-sites, respectively. Values of the empirical parameter R_0 distances were taken from Brown and Altermatt (1985).

The clusters were ranked according to their stability using the difference (Δ) between cation–anion distance, which was estimated from Eq. (1), and the distance equal to the sum of the corresponding effective ion radii (Shannon 1976).

The results of our analysis of the stability of coordinated atomic arrangements around the *W*- and *V*-sites in the studied Li–Al tourmalines are given in Table 2.

IR spectroscopic determination of the arrangements around OH ions

Samples

Two Li–Al tourmalines were selected for IR spectroscopic study of the coordination arrangements surrounding OH^- ions (Table 3). Both tourmalines are characterized by Li/Al atomic ratio close to 1 at the *Y*-site (1.08 и 1.22 for samples 1, 2 respectively) and different Na/Ca atomic ratio at the *X*-site (3.09 and 0.38 for samples 1, 2, respectively). Na-rich tourmaline (sample 1) originated from Eastern Pamirs miarolic pegmatite and Ca-rich tourmaline (sample 2)—from Central Transbaikal. The crystal structures of these tourmalines had already been refined by means of single crystal X-ray structural analysis. Their crystal chemical formulas well agreed with the data of the chemical analyses (Table 3). In case of Na-rich tourmaline (sample 1), hydrogen atoms were localized near the *V*-site.

Powder and oriented single crystal plates were made from samples 1 and 2 for IR spectroscopy investigation. The fine-dispersed powders (grain size of 3–10 μm) were obtained by milling in an agate vial in acetone. Then 20 mg of each sample was mixed with 500 mg of crystalline KBr powder and pressed into a pellet at a vacuum pressure of 1 Pa and a temperature of 100 C. KBr was preliminarily ground and annealed for 3 h at 500 C. This method of pellet preparation guarantees the absence of the absorption bands due to non-structural water in the region 3500–3000 cm^{-1}. Single crystal plates (0.33 mm thick) were cut parallel (∥) and perpendicular (⊥) to the *c* axis.

Table 2 The stability characteristic of triads of octahedra coordinating *W*- and *V*-sites in Li–Al tourmalines

No.	Octahedral triad composition	D_{ij}, Å[a]	$^{W}\Delta$, Å[b]	D_{ij}, Å	$^{W}\Delta$, Å	D_{ij}, Å	$^{W}\Delta$, Å
		Anion at *W*-site					
		$OH^{1.05-}$		$F^{1.0-}$		O^{2-}	
1	$3Li^{+}$	1.85 (1.78)[c]	– 0.28 (0.38)	1.77 (1.71)	– 0.32 (0.38)	1.61 (1.52)	– 0.55 (0.64)
2	$2Al^{3+}$	1.95 (1.95)	0.04 (0.01)	1.86 (1.87)	– 0.01 (0)	1.71 (1.71)	– 0.23 (0.23)
	Li^{+}	2.17 (2.20)	0.04 (0.07)	2.09 (2.13)	0 (0.04)	1.92 (1.73)	– 0.24 (0.43)
3	Al^{3+}	1.82 (1.81)	– 0.09 (0.13)	1.73 (1.73)	– 0.14 (0.14)	1.58 (1.55)	– 0.36 (0.39)
	$2Li^{+}$	2.04 (2.02)	– 0.09 (0.14)	1.96 (1.95)	– 0.13 (0.14)	1.81 (1.73)	– 0.35 (0.43)
4	$3Al^{3+}$	2.04 (2.07)	0.13 (0.16)	1.96 (1.98)	0.09 (0.11)	1.80 (1.78)	– 0.14 (0.16)

Anion at *V*-site					
No	Octahedral triad composition	D_{ij}, Å	$^{V}\Delta$, Å	D_{ij}, Å	$^{V}\Delta$, Å
		$OH^{1.15-}$		O^{2-}	
5	Li^{+}	2.14 (2.13)	0.01 (0)	1.92 (1.87)	– 0.24 (0.29)
	$2Al^{3+}$	1.91 (1.92)	0 (0.01)	1.71 (1.68)	– 0.23 (0.23)
6	Al^{3+}	2.01 (2.03)	0.10 (0.12)	1.80 (1.78)	– 0.14 (0.13)
	$2Al^{3+}$	2.01 (2.03)	0.10 (0.12)	1.80 (1.78)	– 0.14 (0.13)

[a] D_{ij} is the estimated cation–anion distance

[b] Δ is the difference between D_{ij} and an empirical distance equal to the sum of the corresponding effective ionic radii (Shannon 1976)

[c] In brackets are the distances D_{ij} from the work of Hawthorne (2002) and the corresponding Δ to them

Table 3 Characteristics of the studied tourmalines according to data of X-ray single diffraction

Tourmaline	Coefficients in the formula $X_{0\text{-}1}Y_3Z_6[Si_6O_{18}][BO_3]_3V_3W$					Θ°[a]	References
	X	*Y*	*Z*	*V*	*W*		
Na-rich (sample 1)	$Na_{0.68}Ca_{0.22}vac_{0.10}$	$Li_{1.56}Al_{1.44}$	$Al_{5.82}Mn^{3+}_{0.18}$	OH_3	$OH_{0.64}F_{0.36}$	14.9	Rozhdestvenskaya et al. (2005)
Ca-rich[b] (sample 2)	$Ca_{0.65}Na_{0.25}vac_{0.10}$	$Li_{1.65}Al_{1.35}$	Al_6	$(OH)_{2.75}O_{0.25}$	$OH_{0.40}F_{0.60}$	Not determined	Shtukenberg et al. (2007)

[a] Θ° is the angle between the O3–H^{-} vector and the *c* axis

[b] The compositions of the sites were optimized based on the chemical analysis data taking into account the local balance of valences

Experiment

IR spectra of the samples (Figs. 2, 3; Tables 4, 5) in the wavenumber region 3800–3000 cm^{-1} [the region of stretching vibrations of OH^{-} ions (V^{-}_{OH}), and molecules H_2O (V_{H2O})] with resolution ± 0.5 cm^{-1} were obtained on the upgraded double-beam diffraction grating spectrophotometer Specord M80 equipped with an Ni–Cr source, Ebert high-aperture monochromator and vacuum thermoelement as detector was used. A foil diffraction polarizer with a Teflon foil grid sprayed with 1200 str per 1 mm was used.

The recording was performed with a constant purge of the sample cell with dry air to avoid absorption of atmospheric water. To verify that the tourmalines were purified from water molecules in the region of water deformation vibration (1800–1500 cm^{-1}), a special check was run. Samples were measured at various polarization angles (γ). The program SPECTRUM (Sokolov et al. 1983) was used for approximating the spectra with a number of lines whose profiles varied from those of purely Lorenz type to the ones close to Gauss type. All spectral parameters were varied. The addition of a variable coefficient to the line profiles gave the closest match between the experimental and the theoretical envelopes of spectra as well as the most illustrative data on the structural imperfection in real crystals (which causes widening of the lines in the experimental spectra). Computed fits were evaluated by the discrepancy of the experimental and the approximated spectra.

OH band assignment models

Bands of stretching vibration absorption of hydroxyl ions were assigned to specific local cation arrangements around OH^{-} ions in the *W*- and *V*-sites, taking into account the

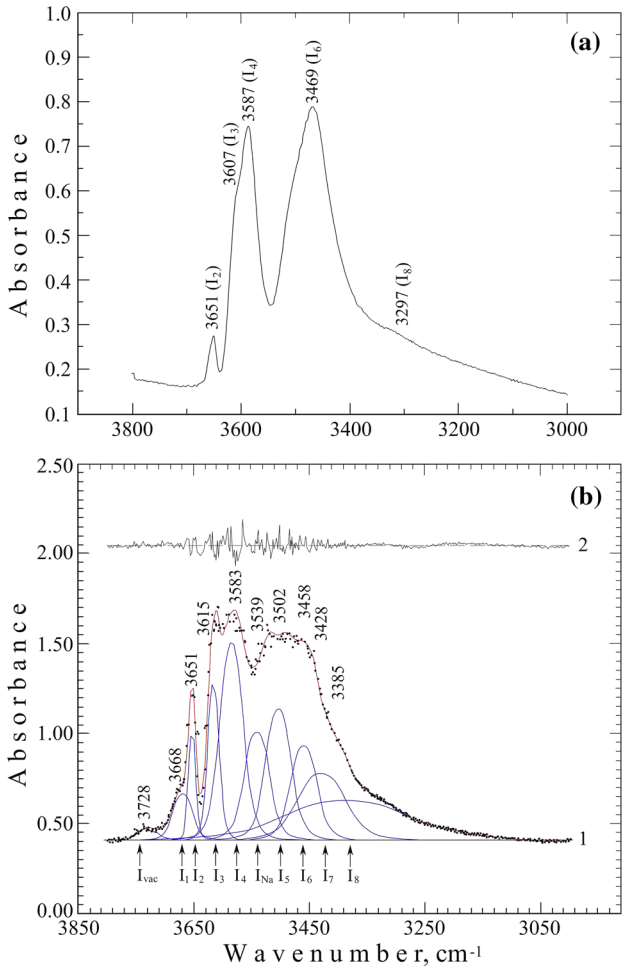

Fig. 2 Examples of Na-rich tourmaline IR spectra (sample 1): **a** powder, **b** single crystal (plate⊥c, γ = 0°) Designations: 1—experimental data; 2—difference curves characterizing magnitude of residuals between experimental and approximated spectra. Symbols of OH^--ion stretching vibration bands match those in Table 4

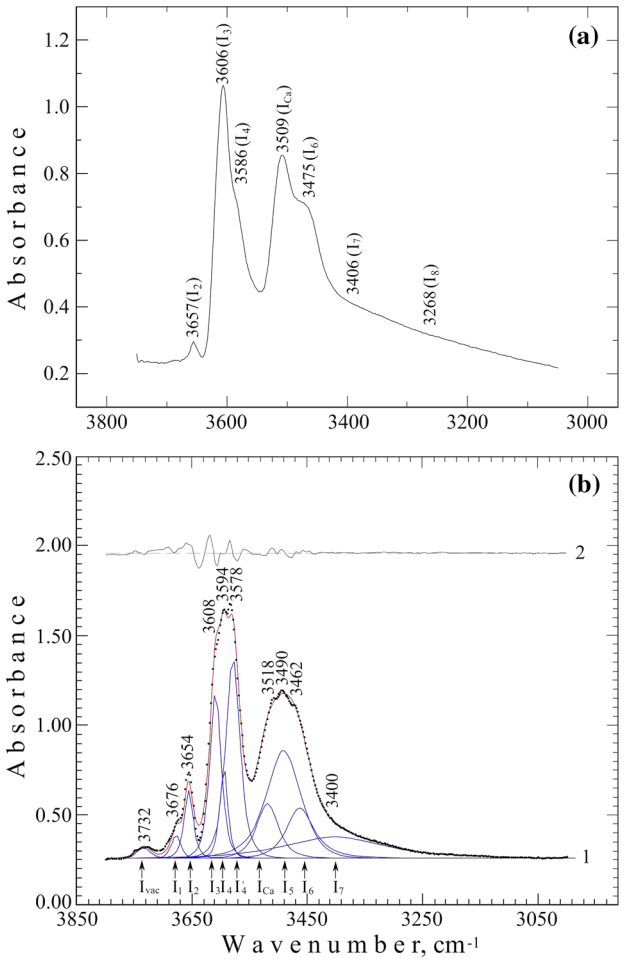

Fig. 3 Examples of Ca-rich tourmaline IR spectra (sample 2): **a** powder, **b** single crystal (plate⊥c, γ = 0°). Designations: 1—experimental data; 2—difference curves characterizing magnitude of residuals between experimental and approximated spectra. Symbols of OH^--ion stretching vibration bands match those in Table 5

stability of $3Y$–$^W(OH^-)$ and $(Y+2Z)$–$^V(OH^-)$ clusters (Table 2), alongside with the results of previous IR spectroscopic studies (Table 1). Also in line with the previous studies (Babushkina et al. 1997; Martínez-Alonso et al. 2002; Bosi 2011), we assumed that the frequency of the stretching of OH^- absorption bands is inversely related to the sum of charges of the cations which coordinate the OH^- group. In addition, a possible shift and split of ν_{OH^-} absorption bands was taken into account. This shift and split could happen as a result of the influence of the cations occupying the *X*-site (of the second coordinated sphere) on the charge balance, which could cause the formation of $3Y$–$^W(OH^-)$–*X* and $(Y+2Z)$–$^V(OH^-)$–*X* clusters.

As a result, a series of assignment models were obtained. The choice between different assignment models was made after comparing the average composition of octahedra around the *V*- and *W*-sites based on IR spectroscopy and X-ray single crystal data. When calculating occupation of octahedral sites using the IR spectra data, we assumed that the ratio between the normalized integral intensities of υOH^- stretching vibration absorption bands was equal to that between the $3Y$–$^W(OH^-)$ or $(Y+2Z)$–$^V(OH^-)$ clusters assigned with these bands. The angle between the *c* axis and the OH band (angle Θ) was used as an additional criterion for choosing the model. When determining the orientation of OH-bond we took into account that when the direction of polarized infrared radiation **E** is parallel with the direction of the OH^- coupling vector (if the angle γ is equal to the angle Θ), the relative intensities of the stretching vibration absorption bands in the IR spectra reach their maximum. The preference was given to the assignment model with angle Θ the value of which was close to that obtained from the X-ray single crystal diffraction data.

Table 4 Positions (cm^{-1}) and integrated intensities of the stretching vibration bands of the hydroxyl ion in the IR spectra of the Na-rich tourmaline (sample 1) and their assignments with the local coordinated arrangements

Band symbol (Fig. 2)	Powder[b]	Single crystal plate					Local arrangement (model 6, Table 6)
		$\perp c$	$\parallel c$				
		Angle $\gamma^{\circ a}$					
		0[b]	0	10	20	30	
I_{vac}	No	3728	3728 (5.0)[c]	3734 (7.4)	3708 (10.8)	3708 (10.0)	^{Y}(LiLiAl)–^{W}(OH) –^{X}vac
I_1	No	3676[d]	3668 (19.4)	3670 (28.2)	3676 (3.0)	3676 (2.1)	^{Y}(LiLiAl)–^{W}(OH)
I_2^e	3651	3650[d]	3651 (16.7)	3650 (31.3)	3656 (16.9)	3656 (19.3)	^{Y}(LiAlAl)–^{W}(OH)
I_3	3607	No	3615 (37.9)	3614 (60.8)	3617 (10.2)	3616 (13.6)	^{Y}Li^{Z}Al^{Z}Al–^{V}(OH)
I_4 [e]	3587[d]	3586[d]	3583 (97.3)	3586 (84.8)	3590 (89.1)	3587 (102.3)	^{Y}Li^{Z}Al^{Z}Al–^{V}(OH)
I_{Na}	No	No	3539 (58.1)	3537 (162.4)	3536 (41.9)	3540 (27.5)	^{Y}Li^{Z}Al^{Z}Al–^{V}(OH)–^{X}Na
I_5	No	No	3502 (70.9)	3480 (79.9)	3495 (65.5)	3508 (55.3)	^{Y}Al^{Z}Al^{Z}Al–^{V}(OH)
I_6^e	3469	3492[d]	3458 (53.1)	3460 (81.6)	3450 (52.6)	3468 (39.7)	^{Y}Al^{Z}Al^{Z}Al–^{V}(OH)
I_7	No	No	3428 (67.3)	3424 (79.2)	3406 (18.9)	3435 (67.9)	O3–H···O5
I_8 [e]	3297	3350	3385 (104.3)	3357 (101.7)	3356 (47.8)	3350 (44.9)	O3–H···O5
I_9	No	No	No	3203 (13.8)	3219 (12.3)	3215 (10.9)	O3–H···O5
I_{10}	No	No	No	No	3081 (4.4)	3079 (3.4)	O3–H···O5

[a]γ-polarization angle

[b]Spectra are presented without decomposition into components

[c]In brackets are the integral intensity of the bands

[d]Bands are asymmetrical

[e]The main bands present in all the IR spectra of Li–Al tourmalines, including those obtained without decomposition (Table 1)

Table 5 Positions (cm^{-1}) and integrated intensities of the stretching vibration bands of the hydroxyl ion in the IR spectra of the Ca-rich tourmaline (sample 2) and their assignments with the local arrangements

Band symbol (Fig. 3)	Powder[b]	Single crystal plate					Local arrangement (model 6, Table 6)
		$\perp c$	$\parallel c$				
		Angle $\gamma^{\circ a}$					
		0[b]	0	10	25	30	
I_{vac}	No	3732	3732 (3.5) [c]	3735 (5.2)	3724 (7.2)	3724 (9.1)	^{Y}(LiLiAl)–^{W}(OH)–^{X}vac
I_1	No	3676[d]	3676 (5.0)	3672 (6.0)	3670 (18.0)	3674 (15.0)	^{Y}(LiLiAl)–^{W}(OH)
I_2^e	3657	3657	3654 (14.5)	3658 (7.0)	3654 (11.0)	3654 (16.0)	^{Y}(LiAlAl)–^{W}(OH)
I_3	3606	3597	3608 (44.0)	3608 (22.0)	3605 (76.0)	3609 (58.0)	^{Y}Li^{Z}Al^{Z}Al–^{V}(OH)
I_4^e	3586[d]	3582[d]	3594 (17.0)	3582 (68.0)	3579 (99.0)	3579 (98.0)	^{Y}Li^{Z}Al^{Z}Al–^{V}(OH)
			3578 (67.0)				
I_{Ca}	3509	3511	3518 (28.0)	3510 (41.0)	3511 (75.0)	3510 (66.0)	^{Y}Li^{Z}Al^{Z}Al–^{V}(OH)–^{X}Ca
I_5	No	No	3490 (88.0)	3480 (39.0)	3470 (60.0)	3482 (98.0)	^{Y}Al^{Z}Al^{Z}Al–^{V}(OH)
I_6^e	3475[d]	3471	3462 (31.0)	3456 (29.0)	3466 (87.0)	3471 (54.0)	^{Y}Al^{Z}Al^{Z}Al–^{V}(OH)
I_7	3406[d]	3400	3400 (51.0)	3397 (6.7)	No	3398 (62.0)	O3–H···O5
I_8^e	3268	3297	No	3325 (14.0)	3324 (21.0)	3328 (6.0)	O3–H···O5
I_9	No	3167	No	3207 (1.9)	3190 (8.4)	3188 (9.1)	O3–H···O5
				3176 (3.0)			O3–H···O5
I_{10}	No	No	No	3066 (3.6)	3058 (5.4)	3068 (8.0)	O3–H···O5

[a]γ-polarization angle

[b]Spectra are presented without decomposition into components

[c]In brackets are the integral intensity of the bands

[d]Bands are asymmetrical

[e]The main bands present in all the IR spectra of Li–Al tourmalines, including those obtained without decomposition (Table 1)

Results and discussion

Stability of the coordinated arrangements around *W*- and *V*-sites based on the bond valence theory

In tourmaline crystal structure, the *W*-site can be occupied by anions OH^-, F^-, and O^{2-}, while the *V*-site can be occupied by anions OH^- and O^{2-}. According to that in Li–Al tourmalines there are may be 12 coordinated arrangements around the *W*-site: ^{Y}(LiLiLi)–^{W}(OH^-, F^-, O^{2-}), ^{Y}(LiLiAl)–^{W}(OH^-, F^-, O^{2-}), ^{Y}(LiAlAl)–^{W}(OH^-, F^-, O^{2-}), ^{Y}(AlAlAl)–^{W}(OH^-, F^-, O^{2-}). According to the previously reported data (Hawthorne 1996, 2002; Bosi 2018), only five of them are stable: ^{Y}(LiLiAl)–^{W}(OH^-, F^-), ^{Y}(LiAlAl)–^{W}(OH^-, F^-) and ^{Y}(AlAlAl)–^{W}(O^{2-}). There may be four coordinated arrangements around the *V*-site: $^{Y}Li^{Z}Al^{Z}Al$–^{V}(OH^-, O^{2-}) and $^{Y}Al^{Z}Al^{Z}Al$–^{V}(OH^-, O^{2-}). Only three of them were stable: $^{Y}Li^{Z}Al^{Z}Al$–^{V}(OH^-), $^{Y}Al^{Z}Al^{Z}Al$–^{V}(OH^-, O^{2-}) (Hawthorne 1996, 2002; Bosi 2018).

Our results on the estimation of the cation–anion bond lengths (Table 2) calculated from formula (*1*) are in line with the already published data. Judging by the difference between D_{ij} and the distances equal to the sum of the corresponding effective ion radii (Shannon 1976), the coordinated clusters range by the degree of stability as follows:

- Around the *W*-site: ^{Y}(LiAlAl)–^{W}(OH^-, F^-) ≫ ^{Y}(LiLiAl)–^{W}(OH^-, F^-) ≈ ^{Y}(AlAlAl)–^{W}(OH^-, F^-, O^{2-}) ≫ ^{Y}(LiLiLi)–^{W}(OH^-, F^-, O^{2-}), ^{Y}(LiAlAl)–^{W}(O^{2-}), ^{Y}(LiLiAl)–^{W}(O^{2-}).
- Around the *V*-site: $^{Y}Li^{Z}Al^{Z}Al$–^{V}(OH^-) > $^{Y}Al^{Z}Al^{Z}Al$–^{V}(OH^-) > $^{Y}Al^{Z}Al\ ^{Z}Al$- ^{V}(O^{2-}) ≫ $^{Y}Li^{Z}Al^{Z}Al$–^{V}(O^{2-}).

Therefore according to our calculation results, the degree of the stability between the clusters ^{Y}(LiLiAl)–^{W}(OH^-, F^-) and ^{Y}(AlAlAl)–^{W}(OH^-, F^-, O^{2-}) is close, though substantially less than that between the clusters ^{Y}(LiAlAl)–^{W}(OH^-, F^-). This does not match with the earlier reported data (Hawthorne 1996, 2002; Bosi 2018). According to our calculation results, arrangements coordinating the *W*-site should be divided into three groups: stable ones ^{Y}(LiAlAl)–^{W}(OH^-, F^-); those on the edge of stability ^{Y}(LiLiAl) – ^{W}(OH^-, F^-), ^{Y}(AlAlAl) – ^{W}(OH^-, F^-, O^{2-}) and unstable ones ^{Y}(LiLiLi)–^{W}(OH^-, F^-, O^{2-}), ^{Y}(LiAlAl)–^{W}(O^{2-}), ^{Y}(LiLiAl)–^{W}(O^{2-}). The received stability estimations of the arrangements coordinating the *V*-site match with the earlier ones very well (Hawthorne 1996, 2002; Bosi 2018): clusters $^{Y}Li^{Z}Al^{Z}Al$–^{V}(OH^-), $^{Y}Al^{Z}Al^{Z}Al$–^{V}(OH^-), $^{Y}Al^{Z}Al^{Z}Al$–^{V}(O^{2-})—stable, cluster $^{Y}Li^{Z}Al^{Z}Al$–^{V}(O^{2-})—unstable.

Short-range arrangements around OH ions according to IR spectroscopy investigation

Infrared spectra description

Na-rich tourmaline (Na/Ca = 3.09) The IR spectrum of Na-rich tourmaline powder sample (sample 1, Table 3) in the region of hydroxyl ion stretching vibration (3800–3000 cm^{-1}) demonstrates four OH bands (Fig. 2a, Table 4): one is of low intensity (3652-3650 cm^{-1}) and two asymmetric wider OH bands are of high intensity (3587–3580 and 3469–3460 cm^{-1}); the fourth one, a wide band of low intensity (3380–3297 cm^{-1}), falls into the stretching vibration region of hydroxyl ions involved in hydrogen bonds. This matches with the results published earlier (Gonzalez-Carreño et al. 1988; Mashkovtsev and Lebedev 1991, Table 1). Four similar bands were also earlier reported in a powder sample spectrum (Castaneda et al. 2000), but the one of the highest intensity (5–9 cm^{-1}) was shifted toward the low-frequency region. A spectrum obtained in the same region from a single crystal plate, cut perpendicular to the *c* axis ($\gamma = 0°$), is actually analogous to the spectrum of the powder sample. The only difference found was the occurrence of low-intensity bands in the high-frequency region (3728, 3676 cm^{-1}). Noteworthy, there is no such band in the published IR spectra acquired the same way (Skogby et al. 2012; Fantini et al. 2013). Nevertheless, in one case (Skogby et al. 2012), the spectrum is entirely analogous to that of our powder sample, while in the other case (Fantini et al. 2013), there is an extra band at 3566 cm^{-1}.

In the IR spectrum obtained from a single crystal Na-rich tourmaline plate cut parallel to the *c* axis, in the region of hydroxyl ions stretching vibration in the range of γ angles from 0° to 30° from 10 to 12 bands appeared (Fig. 2b, Table 4). Four of those bands (I_2, I_4, I_6, I_8) were observed in all non-decomposed spectra. These bands will be further referred to as main bands. The position of the highest-frequency bands I_{vac} and I_1 is close to that of low-intensity bands occurring in the IR spectrum, acquired from a single crystal plate cut perpendicular to the *c* axis. In the stretching vibration region of hydroxyl ions involved in hydrogen bonds, the number of bands varies from 2 to 4.

Ca-rich tourmaline (Na/Ca = 0.38) IR spectra of tourmaline (sample 2, Table 3) are very much like those of sample 1 (Fig. 3, Table 5 and Fig. 2a, b, Table 4, respectively), which is due to the similarity of Li^+/Al^{3+} ratios in *Y* octahedron in the analyzed minerals (Table 3), in other words due to the identically coordinated OH^- ion surrounding. On the powder spectra of Ca-rich tourmaline (sample 2; Fig. 3a) and Na-rich tourmaline (sample 1) occure the following bands: 3657–3651, 3586–3584, 3475–3462 (shifted toward the high-frequency region), 3340–3268 cm^{-1} (shifted toward the low-frequency region). Bands 3586–3584, 3475–3462 cm^{-1}

are as asymmetric as those in the Na-rich tourmaline spectrum. In addition, intensive absorption bands 3610–3604, 3509-3506 and 3406 cm^{-1} show up. Bands 3610–3604, 3509–3506 cm^{-1} were earlier reported for tourmaline spectra of Ca-bearing elbaite (CaO ~ 3 wt; Gonzalez-Carreño et al. 1988; Mashkovtsev and Lebedev 1991, Table 1). The IR spectrum obtained from a single crystal plate cut perpendicular to the *c* axis ($\gamma = 0°$) is analogous to that of a powder sample (Table 5). However, there are two weak bands occurring in the low-frequency region, as in the case of Na-rich tourmaline, in the high-frequency region (3732, 3676 cm^{-1}).

In the IR spectrum, obtained from the single crystal plate cut parallel to the *c* axis, in the range of hydroxyl ion stretching vibration at γ angle varying from 0° to 30°, from 10 to 13 bands appeared (Fig. 3b; Table 5). Bands I_{vac}–I_4, I_5–I_{10} (Table 5) are analogous to those observed in the spectra from sample 1 single crystal plate at angle $\gamma = 0°$. Sample 2 spectra differ from those of sample 1 by the absence of bands in the range 3540–3536 cm^{-1} (I_{Na} Fig. 2b, Table 4) and with the occurrence of a band in the 3518–3508 cm^{-1} range (I_{Ca} Fig. 3b, Table 5). Besides that, in the range of the stretching vibration of hydroxyl ions involved in hydrogen bond, the bands in sample 2 spectra are shifted toward the lower-frequency range.

Therefore, in both Na-rich and Ca-rich tourmaline IR spectra, the locations of hydroxyl ion (coordinated with octahedral cations of the first coordination sphere) stretching vibration bands (I_1–I_4, I_5–I_{10}) are similar. The sharing of the charge balance between cations and vacancies of the second coordinated sphere occupying the *X*-site results not only in a shift and a split of ν_{OH^-} band absorption, corresponding to the first coordinated sphere cations, but also in the appearance of several more bands: $I_{vac} = 3730$–3710 cm^{-1} (in the spectra of samples 1, 2; Figs. 2b, 3b; Tables 4, 5), $I_{Na} = 3540$-3536 cm^{-1} (in the spectra of sample 1; Fig. 2b, Table 4), $I_{Ca.} = 3518$–3508 cm^{-1} (in the spectra of sample 2; Fig. 3b, Table 5).

OH band assignment models

We considered six assignment models for Li–Al tourmalines (Table 6) divided into two groups: in I group (models 1–3) the main bands are assigned as suggested by Mashkovtsev and Lebedev (1991); in II group (models 4–6) the main bands are assigned as suggested by Gonzalez-Carreño et al. (1988). Within the groups the proposed models differed by the ratio of clusters varying in stability and in the location of boundary between the high- and low-frequency regions.

Bands (I_1–I_4, I_5–I_{10}) which are present in both sample spectra were compared to the stable octahedral arrangements of the first coordinated sphere and to hydrogen bonds. Bands of the high-frequency region were assigned to clusters ^{Y}(LiLiAl)–^{W}(OH^-) and ^{Y}(LiAlAl)–^{W}(OH^-); those of low-frequency regions to clusters $^{Y}Li^{Z}Al^{Z}Al$–^{V}(OH^-) and $^{Y}Al^{Z}Al^{Z}Al$–^{V}(OH^-). Cluster ^{Y}(LiLiAl)–^{W}(OH^-), which is located on the edge between the stable and unstable arrangements, was used for getting the ^{Y}[Li/Al] ≈ 1 ratio, as previously done (Mashkovtsev and Lebedev 1991). Skogby et al. (2012) assumed that the value of the ^{Y}[Li/Al] ratio close to 1 can be achieved in the case of the complete short-range order OH^- and F^- ions consistent with the presence of ^{Y}(LiAlAl)–^{W}(OH^-) and ^{Y}(LiLiAl)–^{W}(F^-) clusters. This

Table 6 Models of assignments of stretching vibration bands in Li–Al tourmalines (samples 1, 2) with arrangements coordinating of OH^- ion at *W*- and *V*-sites

Band symbol (Figs. 2, 3)	Models					
	I group			II group		
	1	2	3	4	5	6
I_{vac}	^{Y}(LiLiAl)–^{W}(OH) –^{X}vac					
I_1	^{Y}(LiLiAl)–^{W}(OH)	^{Y}(LiLiAl)–^{W}(OH)	^{Y}(LiLiAl)–^{W}(OH)	^{Y}(LiLiAl)–^{W}(OH)	^{Y}(LiLiAl)–^{W}(OH)	^{Y}(LiLiAl)–^{W}(OH)
I_2	^{Y}(LiLiAl)–^{W}(OH)	^{Y}(LiLiAl)–^{W}(OH)	^{Y}(LiLiAl)–^{W}(OH)	^{Y}(LiLiAl)–^{W}(OH)	^{Y}(LiAlAl) - ^{W}(OH)	^{Y}(LiAlAl)–^{W}(OH)
I_3	^{Y}(LiAlAl)–^{W}(OH)	^{Y}(LiLiAl)–^{W}(OH)	^{Y}(LiLiAl)–^{W}(OH)	^{Y}(LiAlAl)–^{W}(OH)	^{Y}(LiAlAl) - ^{W}(OH)	$^{Y}Li^{Z}Al^{Z}Al$–^{V}(OH)
I_4	^{Y}(LiAlAl)–^{W}(OH)	^{Y}(LiAlAl)–^{W}(OH)	^{Y}(LiAlAl)–^{W}(OH)	$^{Y}Li^{Z}Al^{Z}Al$–^{V}(OH)	$^{Y}Li^{Z}Al^{Z}Al$ - ^{V}(OH)	$^{Y}Li^{Z}Al^{Z}Al$–^{V}(OH)
I_{Na} [a]	$^{Y}Li^{Z}Al^{Z}Al$–^{V}(OH)–^{X}Na			$^{Y}Li^{Z}Al^{Z}Al/^{Y}Al^{Z}Al^{Z}Al$-^{V}(OH)–^{X}Na	$^{Y}Li^{Z}Al^{Z}Al$–^{V}(OH)–^{X}Na	$^{Y}Li^{Z}Al^{Z}Al/^{Y}Al^{Z}Al^{Z}Al$ – ^{V}(OH)–^{X}Na
I_{Ca} [b]	$^{Y}Li^{Z}Al^{Z}Al$–^{V}(OH)–^{X}Ca			$^{Y}Li^{Z}Al^{Z}Al/^{Y}Al^{Z}Al^{Z}Al$ – ^{V}(OH)–^{X}Ca	$^{Y}Li^{Z}Al^{Z}Al$–^{V}(OH)–^{X}Ca	$^{Y}Li^{Z}Al^{Z}Al/^{Y}Al^{Z}Al^{Z}Al$ – ^{V}(OH)–^{X}Ca
I_5	$^{Y}Li^{Z}Al^{Z}Al$–^{V}(OH)	$^{Y}Li^{Z}Al^{Z}Al$–^{V}(OH)	$^{Y}Li^{Z}Al^{Z}Al$–^{V}(OH)	$^{Y}Al^{Z}Al^{Z}Al$–^{V}(OH)	$^{Y}Li^{Z}Al^{Z}Al$ –^{V}(OH)	$^{Y}Al^{Z}Al^{Z}Al$–^{V}(OH)
I_6	$^{Y}Al^{Z}Al^{Z}Al$–^{V}(OH)	$^{Y}Al^{Z}Al^{Z}Al$–^{V}(OH)	$^{Y}Al^{Z}Al^{Z}Al$–^{V}(OH)	$^{Y}Al^{Z}Al^{Z}Al$–^{V}(OH)	$^{Y}Al^{Z}Al^{Z}Al$–^{V}(OH)	$^{Y}Al^{Z}Al^{Z}Al$–^{V}(OH)
I_7	O3–H···O5	O3–H···O5	$^{Y}Al^{Z}Al^{Z}Al$- ^{V}(OH)	O3–H···O5		

[a]Band present only in the spectrum of Na-rich tourmaline (sample 1)

[b]Band present only in the spectrum of Ca-rich tourmaline (sample 2)

assumption could be true only in case of ^{Y}(LiLiAl)–^{W}(F^{-}) arrangements being more stable than ^{Y}(LiLiAl)–^{W}(OH^{-}) arrangements, which contradicts our results (Table 2).

The rest of the stretching vibration bands of hydroxyl ion I_{vac}, $I_{Na,}$ I_{Ca} (Tables 4, 5; Figs. 2, 3) were assigned to cations and vacancies in *X*-site. According to Fantini et al. (2013), high-frequency band I_{vac} = 3730–3710 cm^{-1} was assigned to the bond ^{Y}(LiLiAl)–^{W}(OH^{-})–^{X}vac in both Na-rich and Ca-rich tourmaline spectra, while low-frequency band I_{Na} = 3540–3536 cm^{-1}, appearing only in sample 1 spectrum, was assigned to the bond ^{Y}Li^{Z}Al^{Z}Al–^{V}(OH^{-})–^{X}Na^{+}. Using the same principle, the band I_{Ca} = 3518–3508 cm^{-1} was assigned to the bond ^{Y}Li^{Z}Al ^{Z}Al–^{V}(OH^{-})–^{X}Ca^{2+}. As the Na-rich tourmaline contains a calcium admixture (Table 3) and the Ca-rich tourmaline contains a sodium admixture (Table 3) it is possible that the positions of bands I_{Na} and I_{Ca} depend on the Na^{+}/Ca^{2+} ratio and correspond to ^{Y}Li^{Z}Al^{Z}Al–^{V}(OH^{-})–^{X}(Na^{+}, Ca^{2+}).

The comparisons between average octahedron (coordinating OH^{-} ions in the *V*- and *W*-sites) compositions, based on the data of IR spectroscopic and X-ray structural analyses, enabled eliminating three models 1, 4, and 5 ($0.05 \le {}^{W}\Delta \le 0.11$ и $0.03 \le {}^{V}\Delta \le 0.08$) all at once. Moreover after taking into account the value of hydrogen bond O3–H···O5 angle obtained from the X-ray single crystal structure data, model 2 was rejected as well, because the Θ values in case of sample 2 varied from 1.51 to 8.08° (Table 3), though they cannot be lower than 10° according to $^{V}\Delta$ values (Table 7). Therefore, at this stage only two models, 3 and 6, may be considered to represent a united model for describing short-range order in the studied Li–Al tourmalines.

In the low-frequency region, the average maximum value of integral intensity of OH-ion stretching bands (I_3, I_4, I_5, I_6; Table 4) which were previously assigned to clusters $(Y+2Z)$–^{V}(OH^{-}) increases in the range of angles γ from 0° to 10° and then decreases at angles γ > 10° (Table 4). Consequently, according to the data of IR spectroscopy, Θ angle value proved to be close to 10°. But in model 3, the average occupation of octahedra coordinating *V*-site is close to those obtained by X-ray single crystal diffraction but only at γ = 20° ($^{V}\Delta \le 0.01$ apfu, Table 7), which contradicts the Θ angle value estimated from the average maximum value of the integrated intensity of the bands on the IR spectra. In model 6, the occupation of octahedra coordinating *V*-site is close to that obtained by X-ray single crystal diffraction at

Table 7 Comparison the average composition of octahedra coordinating OH^{-} ions at *W*- and *V*-sites obtained by main assignment models (single crystal plate) and by X-ray single diffraction

γ°[a]	Na-rich tourmaline (sample 1)				Ca-rich tourmaline (sample 2)			
	$3Y - {}^{W}(OH)_{0.64}$	$^{W}\Delta$, Å[c]	$(Y+2Z) - {}^{V}(OH)_{1.00}$	$^{V}\Delta$, Å[c]	$3Y - {}^{W}(OH)_{0.30}$	$^{W}\Delta$, Å[c]	$(Y+2Z) - {}^{V}(OH)_{0.92}$	$^{V}\Delta$, Å[c]
Model 2								
0	$Li_{0.31}Al_{0.33}$	− 0.02	$Li_{0.19}Al_{0.81}$	+0.02	$Li_{0.14}Al_{0.16}$	− 0.03	$Li_{0.22}Al_{0.70}$	+ 0.05
10	$Li_{0.34}Al_{0.30}$	+ 0.01	$Li_{0.16}Al_{0.84}$	-0.01	$Li_{0.14}Al_{0.16}$	− 0.04	$Li_{0.17}Al_{0.75}$	+ 0
20	$Li_{0.27}Al_{0.37}$	− 0.06	$Li_{0.18}Al_{0.82}$	+0.01	$Li_{0.15}Al_{0.15}$	− 0.02	$Li_{0.12}Al_{0.80}$	−0.05
30	$Li_{0.27}Al_{0.37}$	− 0.06	$Li_{0.19}Al_{0.81}$	+0.02	$Li_{0.15}Al_{0.15}$	− 0.02	$Li_{0.19}Al_{0.73}$	+ 0.02
Boundary[b]	I_4–I_7 3590–3470 cm^{-1}							
Model 3								
0	$Li_{0.31}Al_{0.33}$	− 0.02	$Li_{0.12}Al_{0.88}$	− 0.05	$Li_{0.14}Al_{0.16}$	− 0.03	$Li_{0.16}Al_{0.76}$	− 0.01
10	$Li_{0.34}Al_{0.30}$	+ 0.01	$Li_{0.11}Al_{0.89}$	− 0.06	$Li_{0.13}Al_{0.17}$	− 0.04	$Li_{0.16}Al_{0.76}$	− 0.01
20	$Li_{0.27}Al_{0.37}$	− 0.06	$Li_{0.16}Al_{0.84}$	− 0.01	$Li_{0.15}Al_{0.15}$	− 0.02	$Li_{0.11}Al_{0.81}$	− 0.06
30	$Li_{0.27}Al_{0.37}$	− 0.06	$Li_{0.11}Al_{0.89}$	− 0.06	$Li_{0.15}Al_{0.15}$	− 0.02	$Li_{0.14}Al_{0.78}$	− 0.03
Boundary	I_4–I_7 3590–3470 cm^{-1}							
Model 6								
0	$Li_{0.33}Al_{0.31}$	+ 0	$Li_{0.17}Al_{0.83}$	+ 0	$Li_{0.13}Al_{0.17}$	− 0.04	$Li_{0.16}Al_{0.76}$	− 0.01
10	$Li_{0.31}Al_{0.33}$	− 0.02	$Li_{0.16}Al_{0.84}$	− 0.01	$Li_{0.15}Al_{0.15}$	− 0.02	$Li_{0.17}Al_{0.75}$	+ 0
20	$Li_{0.24}Al_{0.40}$	− 0.09	$Li_{0.15}Al_{0.85}$	− 0.02	$Li_{0.16}Al_{0.14}$	− 0.01	$Li_{0.17}Al_{0.75}$	+ 0
30	$Li_{0.23}Al_{0.41}$	− 0.10	$Li_{0.18}Al_{0.82}$	+ 0.01	$Li_{0.15}Al_{0.15}$	− 0.02	$Li_{0.15}Al_{0.77}$	− 0.02
Boundary	I_2–I_3 3658–3605 cm^{-1}							
X-ray diffraction data	$Li_{0.33}Al_{0.31}$		$Li_{0.17}Al_{0.83}$		$Li_{0.17}Al_{0.13}$		$Li_{0.17}Al_{0.75}$	

[a] γ is polarization angle

[b] boundary between high and low-frequency region in the IR spectrum

[c] $^{W}\Delta$ is the difference between the content of Li^{+} ions in the *Y*- site according to IR spectroscopy and X-ray diffraction data

$^{V}\Delta$ is the difference between the content of Li^{+} ions in the *Y*-site according to IR spectroscopy and X-ray diffraction data

γ value from 0° to 30° ($^{V}\Delta \leq 0.02$ apfu, Table 7) which does not contradict the Θ angle value estimated from the average maximum value of the integrated intensity of the bands on the IR spectra. This makes model 6 preferable due to its angle between O3–H^- vector and the *c* axis direction lying in the interval $0° < \Theta < 20°$, which is similar to the X-ray single crystal diffraction data obtained from the refinement of crystal structure of sample 1 ($\Theta = 14.9°$, Table 3).

The close match between the average compositions of octahedra coordinating OH^- ions in the studied samples, proven by X-ray diffraction and IR spectroscopy data (model 6) in a wide range of angles of polarization angle γ (Table 7), indicate the probability of a disordered distribution of protons resulting from the growth of desymmetrization (Shtukenberg et al. 2007).

The region of stretching vibration of hydroxyl ion involved in hydrogen bonds (I_7–I_{10} 3435–3058 cm^{-1}) is rather complicated to interpret because it may include some overtones and component frequencies of other tourmaline vibrations.

Short-range order in tourmaline with ^{Y}[Li/Al] ratio ≈ 1

The results of the comprehensive study allowed describing short-range order in Li–Al– (OH^-, F^-) tourmalines, which is controlled by the bond valence theory and does not contradict with occupancies of crystallographic sites determined by single crystal X-ray diffraction method.

As follows from the selected unified assignment model (Tables 4, 5, 7), OH^- ions surrounding the *W*-site in the studied Li–Al tourmalines (sample 1, 2) are presented by the following $3Y$–$^{W}(OH^-)$ clusters: ^{Y}(LiAlAl)–$^{W}(OH^-)$, ^{Y}(LiLiAl)–$^{W}(OH^-)$. OH^- ions surrounding the *V*-site are represented by clusters $(Y+2Z)$–$^{V}(OH^-)$: $^{Y}Li^{Z}Al^{Z}Al$–$^{V}(OH^-)$ and $^{Y}Al^{Z}Al^{Z}Al$–$^{V}(OH^-)$. In Ca-rich tourmaline (sample 2), except for the clusters $(Y+2Z)$–$^{V}(OH^-)$, there are insignificant amounts (in the ratio 1:11) of clusters $(Y+2Z)$–$^{V}(O^{2-})$.

According to our calculations, the stability of the clusters ^{Y}(LiAlAl)–$^{W}(OH^-)$, ^{Y}(LiAlAl)–$^{W}(F^-)$ and ^{Y}(LiLiAl)–$^{W}(OH^-)$, ^{Y}(LiLiAl)–$^{W}(F^-)$ are close (Table 2). This lets us assume that F^- ions surrounding the *W*-site in the studied Li–Al tourmalines is represented by $3Y$–$^{W}(F^-)$ clusters: ^{Y}(LiAlAl)–$^{W}(F^-)$, ^{Y}(LiLiAl)–$^{W}(F^-)$. Since the *W*-site in the investigated tourmalines is split due to the tendency of OH^- and F^- anions to ordered distribution (Rozhdestvenskaya et al. 2005). So, the $3Y$- $^{W}(OH^-)$ and $3Y$–$^{W}(F^-)$ clusters are orderly distributed. According to *W*-site occupation of the studied tourmalines (Table 3), the ratio between the $3Y$–$^{W}(OH^-)$ and $3Y$–$^{W}(F^-)$ clusters is equal to 1.8 and 0.67 for the Na-rich (sample 1) and Ca-rich (sample 2) tourmalines, respectively. According to *Y*-site occupancies (Table 3), the ratio between statistically distributed ^{Y}(LiLiAl)–*W*, ^{Y}(LiAlAl)–*W* and ($^{Y}Li^{Z}Al^{Z}Al$)–$^{V}(OH^-)$, ($^{Y}Al^{Z}Al^{Z}Al$)–$^{V}(OH^-)$ clusters equals to 1.06 and 1.31 for the Na-rich (sample 1) and Ca-rich (sample 2) tourmalines, respectively.

Based on the proposed unified assignment model (Table 4, 5), we can suggest the presence of larger clusters $3Y$–*W*–*X* and $(Y+2Z)$–*V*–*X* in the studied Li–Al tourmalines: ^{Y}(LiLiAl)–$^{W}(OH^-)$–^{X}vac (cluster ^{Y}(LiLiAl)–$^{W}(F^-)$–^{X}vac is also possible), ($^{Y}Li^{Z}Al^{Z}Al$)–$^{V}(OH^-)$–$^{X}Na^+$, ($^{Y}Li^{Z}Al^{Z}Al$)–$^{V}(OH^-)$–$^{X}Ca^{2+}$. According to *X*-site occupancy (Table 3) the ratio between the ^{Y}(LiLiAl)–$^{W}(OH^-, F^-)$–^{X}vac, ($^{Y}Li^{Z}Al^{Z}Al$)–$^{V}(OH^-)$–$^{X}Na^+$ and ($^{Y}Li^{Z}Al^{Z}Al$)–$^{V}(OH^-)$–$^{X}Ca^{2+}$ clusters is equal to 1:6.8:2.2 and 1:2.5:6.5 for the Na-rich (sample 1) and Ca-rich (sample 2) tourmalines, respectively. In the Na-rich tourmaline cluster ($^{Y}Li^{Z}Al^{Z}Al$)–$^{V}(OH^-)$–$^{X}Na^+$ is dominant, while in the Ca-rich, $^{Y}Li^{Z}Al\ ^{Z}Al$– $^{V}(OH^-)$–$^{X}Ca^{2+}$ is dominant.

Conclusion

Integrating the arguments of bond valence theory and experimental approaches of IR spectroscopy and X-ray diffraction analysis, the short-range order in Li–Al–(OH^-, F^-) tourmalines with $^{Y}[Li/Al] \approx 1$ and different atomic Na^+/Ca^{2+} ratio was studied.

The stability of atomic arrangements coordinating *W*- and *V*-sites occupied by OH^-, F^- and O^{2-} ions is refined on the base of bond valence theory. For the first time, a unified assignment model of absorption bands in the region of OH^--ion stretching vibrations in IR spectra of Li–Al tourmalines controlled by the bond valence theory is proposed which does not contradict the long-range order. The results obtained by a wide range of methods allow to determine the types of coordinated atomic arrangements around the *W*- and *V*-sites (OH^- and F^- ions) in the structure of studied tourmalines, to analyze their ratio and distribution. It was shown that coordinated arrangements around the *W*- and *V*-sites in the tourmaline structure can have an ordered or a random distribution.

Acknowledgements This work was supported by the President of Russian Federation grant for leading scientific schools (No. NSh-3079.2018.5).

References

Babushkina MS, Nikitina LP, Ovchinnikov NO (1997) The composition and structure characteristics of phlogopite lamproites Kostomukshi. ZVMO 2:71–84 **(in Russian)**

Bosi F (2011) Stereochemical constraints in tourmaline: from a shortrange to a long-range structure. Can Mineral 49:17–27

Bosi F (2018) Tourmaline crystal chemistry. Am Mineral 103:298–306

Bosi F, Skogby H, Balicr-Žunicr T (2016) Thermal stability of extended clusters in dravite: a combined EMP, SREF and FTIR study. Phys Chem Miner 43:395–407

Brown ID (2002) The chemical bond in inorganic chemistry: the bond valence model. Oxford University Press, Oxford, p 372

Brown ID, Altermatt D (1985) Bond-valence parameters obtained from a systematic analysis of the inorganic crystal structure database. Acta Cryst B 41:244–247

Buerger MJ, Parrish W (1937) The unit cell and space group of tourmaline. Am Mineral 22:1139–1150

Castañeda C, Oliveira EF, Gomes N, Soares ACP (2000) Infrared study of OH in tourmaline from the elbaite-schorl series. Am Mineral 85:1503–1507

Ertl A, Hughes JM, Pertlik F, Foit FF Jr, Wright SE, Brandstätter F, Marler B (2002) Polyhedron distortions in tourmaline. Can Mineral 40:153–162

Fantini C, Tavares MC, Krambrock K, Moreira RL, Righi A (2013) Raman and infrared study of hydroxyl sites in natural uvite, fluoruvite, magnesio-foitite, dravite and elbaite tourmalines. Phy Chem Miner 21:811–816

Gatta GD, Bosi F, McIntyre GJ, Skogby H (2014) First accurate location of two proton sites in tourmaline: a single-crystal neutron diffraction study of oxy-dravite. Mineral Mag 78(3):681–692

Gebert W, Zemann J (1965) Messung des Ultrarot-Pleochroismus von Mineralen II. Der Pleochroismus der OH-Streckfrequenz in Turmalin. Neues Jahrb Mineral Monatsh 8:232–235

Gonzalez-Carreño T, Fernandez M, Sanz J (1988) Infrared and electron microprobe analysis of tourmalines. Phy Chem Miner 15:452–460

Gorskaya MG, Frank-Kamenetskaya OV, Rozhdestvenskaya IV, Frank-Kamenetskii VI (1982) Refinement of the crystal structure of Al-rich elbaite and some aspects of the crystal chemistry of tourmalines. Sov. Phys. Crystallogr 27:63–66

Hallsworth CR, Chisholm JI (2008) Provenance of Late Carboniferous sandstones in the Pennine Basin (UK) from combined heavy mineral, garnet geochemistry and palaeocurrent studies. Sed Geol 203:196–212

Hawthorne FC (1996) Structural mechanisms for light-element variations in tourmaline. Can Mineral 34:123–132

Hawthorne FC (2002) Bond-valence constraints on the chemical composition of tourmaline. Can Mineral 40:789–797

Henry DJ, Guidotti CV (1985) Tourmaline as a petrogenetic indicator mineral: an example from the staurolite-grade metapelites of NW Maine. Am Mineral 70:1–15

Kuzmin VI, Dobrovolskaya NV, Solntzeva LS (1979) Tourmaline and its use in prospecting and evaluation work. Nedra, Moscow, p 286 (**in Russian**)

Kuznetsova LG, Zolotarev AA, Frank-Kamenetskaya OV, Rozhdestvenskaya IV, Bronzova YuM, Spratte J, Ertl A (2011) Chemical composition and species attribution of tourmalines from a rare-metal pegmatite vein with scapolite, Sangilen Upland. Tuva. Geology of Ore Deposits 53(8):806–817

Martínez-Alonso S, Rustad JR, Goetz AFH (2002) Ab initio quantum mechanical modeling of infrared vibrational frequencies of the OH group in dioctahedral phyllosilicates. Part II: main physical factors governing the OH vibrations. Am Mineral 87:1224–1234

Mashkovtsev RI, Lebedev AS (1991) IR-spectroscopy of OH-groups in tourmaline. Soviet Geol Geophys 32:80–84

Nikolskaya LV, Samoylovich MI (1977) Optical spectra of tourmaline in the near infrared region (1000–2500 nm). Report USSR Acad Sci 232(5):1185–1188 **(in Russian)**

Pauling L (1929) The principles determining the structure of complex ionic crystals. J Am Chem Soc 51:1010–1026

Rozhdestvenskaya IV, Frank-Kamenetskaya OV, Zolotarev AA, Bronzova YuM, Bannova II (2005) Refinement of the crystal structures of three fluorine-bearing elbaites. Cryst Rep 50:907–913

Rozhdestvenskaya IV, Frank-Kamenetskaya OV, Kuznetsova LG, Bannova II, Bronzova YuM (2007) Refinement of the Crystal Structure of Lithium-Bearing Uvite. Cryst Rep 52:227–231

Rozhdestvenskaya IV, Bronzova YuM, Frank-Kamenetskaya OV, Zolotarev AA, Kuznetsova LG, Bannova II (2008) Refinement of the Crystal Structure of Calcium–Lithium–Aluminum Tourmaline from the Pegmatite Vein in the Sangilen Upland (Tuva Republic). Cryst Rep 53:250–254

Shannon RD (1976) Revised effective ionic radii and systematic studies of interatomic distances in halides and chalcogenides. Acta Cryst 32:751–767

Shtukenberg AG, Rozhdestvenskaya IV, Frank-Kamenetskaya OV, Bronzova JM, Euler H, Kirfel A, Bannova II, Zolotarev AA (2007) Symmetry and crystal structure of biaxial elbaite–liddicoatite tourmaline from the Transbaikalia region, Russia. Am Mineral 92:675–686

Skogby H, Bosi F, Lazor P (2012) Short-range order in tourmaline: a vibrational spectroscopic approach to elbaite. Phy Chem Miner 39:811–816

Sokolov, Yu A, Novikov GV (1983) Decomposition into components of Mössbauer spectra and X-ray diffraction patterns. IEM Preprint 25, Chernogolovka, p 32 (**in Russian**)

van Hinsberg VJ, Henry DJ, Marschall HR (2011) Tourmaline: an ideal indicator of its host environment. Can Mineral 49:1–16

Vďačný M, Bacik P (2015) Provenance of the Permian Malužiná Formation sandstones (Malé Karpaty Mountains, Western Carpathians): evidence of garnet and tourmaline mineral chemistry. Geol Carpath 66(2):83–97

Vereshchagin OS, Rozhdestvenskaya IV, Frank-Kamenetskaya OV, Zolotarev AA (2014) Ion substitutions and structural adjustment in Cr-bearing tourmalines. Eur J Min 26(2):309–321

Vereshchagin OS, Khudoley AK, Ershova VB, Prokopiev AV, Schneider GV (2018) Provenance of Jurassic-Cretaceous siliciclastic rocks from the northern Siberian Craton: an integrated heavy mineral study. J Geosci 63:199–213

Watenphul A, Schlüter J, Bosi F, Skogby H, Malcherek T, Mihailova B (2016) Influence of the octahedral cationic-site occupancies on the framework vibrations of Li-free tourmalines, with implications for estimating temperature and oxygen fugacity in host rocks. Am Mineral 101:970–985